• RESEARCH PAPER •

Equivalent input disturbance-based load frequency control for smart grid with air conditioning loads

Li Jin[1,2,3,4], Yong He[1,2,4*], Chuan-Ke Zhang[1,2,4], Xing-Chen Shangguan[1,2,3,4], Lin Jiang[3] & Min Wu[1,2,4]

[1]*School of Automation, China University of Geosciences, Wuhan* 430074*, China;*
[2]*Hubei Key Laboratory of Advanced Control and Intelligent Automation for Complex Systems, Wuhan* 430074*, China;*
[3]*Department of Electrical Engineering and Electronics, University of Liverpool, Liverpool* L69 3GJ*, United Kingdom;*
[4]*Engineering Research Center of Intelligent Technology for Geo-Exploration, Ministry of Education, Wuhan* 430074*, China*

Abstract Integrating intermittent wind power into power systems results in low or zero inertia, threatening their frequency stability. To accommodate intermittent generations, the demand response (DR) is introduced, and air conditioning loads (ACs) account for an increasing proportion of all loads. The replacement of traditional generators with wind turbines and the ACs user uncertainties produce parameter uncertainties. This paper aims to construct an equivalent input disturbance (EID)-based load frequency control (LFC) strategy for the power system by considering wind power and ACs. First, an open-loop model is constructed for the LFC scheme with parameter uncertainties. Then, the parameter uncertainties and external disturbance are lumped into a fictitious disturbance, which is estimated using an EID estimator. By incorporating the estimation of disturbance into the control input, the disturbance-rejection performance is achieved. Next, the Lyapunov theory is used to derive the two linear-matrix-inequality-based asymptotic stability criteria. A design algorithm is developed for the EID-based LFC scheme by exploiting an overall performance evaluation index. Finally, simulation results for the one-area and two-area LFC schemes show that, compared with the existing approaches, the method presented realizes the better disturbance rejection and higher robustness against parameter uncertainties, wind power fluctuation, and tie-line power changes. Additionally, its robustness to time delays is verified.

Keywords Equivalent input disturbance, Load frequency control, Parameter uncertainties, Wind power, Air conditioning loads

1 Introduction

Load frequency control (LFC) maintains the frequency of each control area and regulates the tie-line power flows between neighboring control areas [1, 2]. The increasing penetration of intermittent wind power reduces the usage of the traditional generations that are costly and environmentally unfriendly [3, 4]. Meanwhile, replacing conventional generators with wind turbines leads to low or zero inertia in the LFC system. Thus, by contributing to a reduction of the system's inertia response, a high wind power penetration level can endanger the stable operation of the system [5, 6]. Energy storage shows great promise for balancing generation and demand, while large storage devices have a low-efficiency and high-cost [7]. Hence, real-time smart responsive load participation, known as demand response (DR), has been an alternative method for balancing the demand and supply, i.e., when the frequency of the power system

* Corresponding author (email: heyong08@cug.edu.cn)

fluctuates, the load aggregator changes the working state of the participating DR resources following the dispatching instruction to suppress the frequency fluctuation [8]. Conventionally, most dynamic demand control employs the thermostatically controlled appliances, and air conditioning loads (ACs) account for a large proportion of all loads [9, 10]. There are many approaches about using the ACs for assisting frequency regulation, e.g., the load frequency modulation model based method [11], direct load control based optimal dispatch strategy [12], collaborative control strategy [13], and transfer function based PID control [14]. Nevertheless, most of the literatures focus on how to control the ACs based on the idea of optimization. Moreover, the ACs users' flexible participation often allows the power system to operate at uncertain conditions, which combines the inertia reduced by introducing wind power into a conventional power system, leading to parameter uncertainties [15, 16]. However, only a few studies investigate the application of robust techniques to addressing these parameter uncertainties and external disturbance in the wind power system with the ACs participation.

Many robust control techniques are proposed to improve the stability of power systems in the presence of parameter uncertainties and external disturbances, e.g., the H_∞ control [10, 17], sliding model control [18], $\mu-$synthesis [19], decay-rate based control [20], and fuzzy control [21, 22]. These techniques address the influence of disturbances and uncertainties using a feedback control system. They are referred as one-degree of freedom control structures where some design constraints are required, including the trade-off between the dynamic performance and robustness [23].

On the other hand, the disturbance and uncertainty estimation and attenuation (DUEA) methods release these constraints. The two-degree of freedom control mode is employed, i.e., the outer loop is designed for eliminating tracking errors, and the inner loop is responsible for rejecting the disturbances. By estimating the disturbance from measurable variables, a control action is then taken based on the disturbance estimate to compensate for the influence of the disturbance [24]. As a classical DUEA method, the active disturbance rejection control (ADRC) is proposed to compensate for the non-modeled uncertainties [25, 26] or the periodic load in wind turbines [27]. The equivalent input disturbance (EID)-based approach is very effective for reducing the effect of the disturbances on the output while requiring none of the inverse dynamics of the plant model and avoiding the cancellation of unstable poles and zeroes for a nonminimum-phase plant [28, 29]. This method is used to enhance the tracking performance of the power system integrated with wind power [30]. Furthermore, many improved EID-based methods are proposed to realize better dynamic performances on eliminating tracking errors [31, 32]. However, these approaches remain to be exploited for designing a robust control strategy for the smart grid integrated with both wind power and ACs participation.

This paper aims to develop an EID-based LFC scheme that has robust performance against the parameter uncertainties and external disturbance arising from the smart grid with ACs participating in regulating the frequency. First, an open-loop state-space model is established with parameter uncertainties for the LFC scheme considering wind power and ACs. Then, the parameter uncertainties and external disturbance are lumped together to form a fictitious disturbance variable and are estimated using an EID estimator constructed with the Luenberger state observer. The inverse of the estimated EID is imposed on the control input channel to compensate for the influence of parameters uncertainty and external disturbance on the output. Next, a closed-loop LFC scheme equipped with an EID-based controller is modelled by two subsystems equivalently. That is, one subsystem contains the state feedback controller while the other subsystem includes the EID estimator. Through the Lyapunov theory, two stability conditions are established to obtain these two controllers, while guaranteeing the asymptotic stability of the LFC scheme based on the separation theorem [33]. This approach simplifies the solution process in [30] where the Riccati equation and pole placement method are recalled. Compared with the existing methods, the developed EID-based controller is demonstrated to have increased disturbance-rejection capability and robustness to parameter uncertainties, random wind power changes, and load demands. Moreover, the simulation results show that, when time delays arise in the LFC communication channels and ACs participation loop [34], the EID-based LFC controller designed without considering time delay remains effective in eliminating tracking errors.

The remainder of this paper is organized as follows. In Section 2, the open-loop model of the LFC

scheme is discussed at first considering wind power and the ACs. Then, a full order state observer is designed to estimate the disturbance. In Section 3, by using the Lyapunov theory, a robust LFC strategy with the EID-based controller is investigated. Case studies are conducted in Section 4 to verify the effectiveness and improvements of the proposed method. Finally, the conclusion is given in Section 5.

2 Dynamic model of the LFC scheme

For the multi-area LFC scheme integrated with wind power and the modular of ACs, this section constructs an open-loop model with parameter uncertainties. Then, by lumping the external disturbance and the parameter uncertainties into a fictitious disturbance variable, an EID estimator is utilized to estimate the influence of the combined disturbance on the output. Based on the estimation results, the inverse of the estimated EID is added into the control input such that the LFC scheme realizes disturbance-rejection performance effectively.

2.1 Model of LFC scheme with wind power power and ACs

The structure of area i involved with an EID-based controller is configured in Figure 1 where $\Delta f_i, \Delta P_{tie-i}$, $\Delta P_{mi}, \Delta P_{vi}$, ΔP_{wi}, ΔP_{Wi}, and ΔP_{aci} are the deviation of frequency, tie-line power exchange, mechanical output of generator, valve position, wind power, output of wind turbine generator, and ACs, respectively; M_i, D_i, T_{gi}, T_{ti}, R_{ni}, and T_{Wi} are the moment of inertia of generator unit, generator unit damping coefficient, time constant of the governor, time constant of the turbine, speed drop, and time constants of the wind turbine generator, respectively; T_{ij} is the tie-line synchronizing coefficient between area i and area j; β_i is the frequency bias factor; d_{aci} and $k_{aci} = \frac{m_i c_{pi} k}{EER}$ are the damping coefficient and combined integral gain, respectively; m_i, c_{pi}, k, and EER donate the mass of air flow, specific heat capacity of the air, gain factor in the smart thermostat, and energy efficiency ratio, respectively.

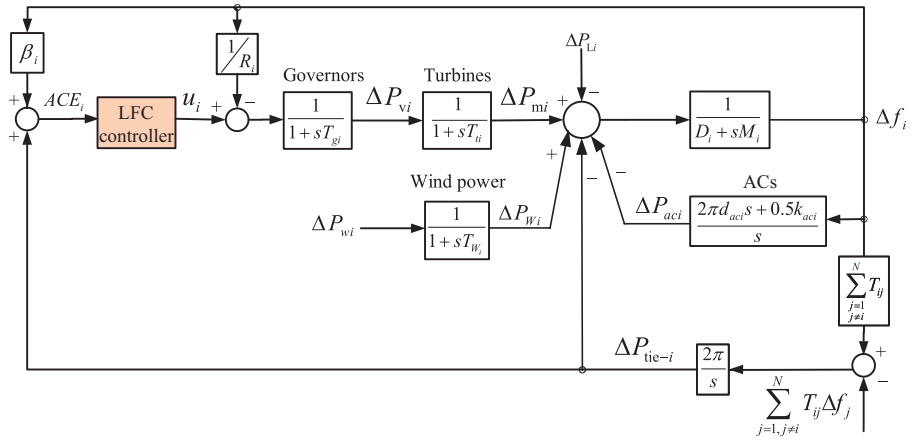

Figure 1 EID-based LFC structure (single-area LFC: without tie-line power exchange ΔP_{tie-i}; multi-area LFC: with tie-line power exchange ΔP_{tie-i})

For the multi-area LFC scheme, the area control error (ACE) of area i is given as

$$ACE_i = \beta_i \Delta f_i + \Delta P_{tie-i}$$

For the single-area LFC scheme without the tie-line power exchanges between adjacent areas, the ACE is defined in below

$$ACE = \beta \Delta f$$

Define the following notations

$$x_i = [\Delta f_i, \Delta P_{tie,i}, \Delta P_{mi}, \Delta P_{vi}, \Delta P_{Wi}, \Delta P_{aci}]^T, w_i^T = \left[\Delta P_{Li}, \sum_{j=1, j\neq i}^{N} T_{ij}\Delta f_j, \Delta P_{wi}\right], y_i = ACE_i.$$

The open-loop model of area i in the LFC schemes is obtained as

$$\begin{cases} \dot{x}_i(t) = A_i x_i(t) + B_i u_i(t) + F_i \omega_i(t) \\ y_i(t) = C_i x_i(t) \end{cases} \tag{1}$$

where

$$A_i = \begin{bmatrix} -\frac{D_i}{M_i} & -\frac{1}{M_i} & \frac{1}{M_i} & 0 & \frac{1}{M_i} & -\frac{1}{M_i} \\ 2\pi \sum_{j=1, j\neq i}^{N} T_{ij} & 0 & 0 & 0 & 0 & 0 \\ 0 & 0 & -\frac{1}{T_{ti}} & \frac{1}{T_{ti}} & 0 & 0 \\ -\frac{1}{R_i T_{gi}} & 0 & 0 & -\frac{1}{T_{gi}} & 0 & 0 \\ 0 & 0 & 0 & 0 & -\frac{1}{T_W i} & 0 \\ 0.5k_{aci} - D_{aci}D_i & -D_{aci} & D_{aci} & 0 & D_{aci} & -D_{aci} \end{bmatrix}, B_i = \begin{bmatrix} 0 \\ 0 \\ 0 \\ \frac{1}{T_{gi}} \\ 0 \\ 0 \end{bmatrix}, F_i = \begin{bmatrix} -\frac{1}{M_i} & 0 & 0 \\ 0 & -2\pi & 0 \\ 0 & 0 & 0 \\ 0 & 0 & 0 \\ 0 & 0 & \frac{1}{T_W i} \\ -D_{aci} & 0 & 0 \end{bmatrix}$$

$$C_i = [\beta_i \ 1 \ 0 \ 0 \ 0 \ 0], \beta_i = R_i + D_i, D_{aci} = \frac{2\pi d_{aci}}{M_i}$$

For simplicity, in system (1), coefficient matrices A_i, B_i, C_i, and F_i are rewritten with A, B, C, and B_d, respectively. We have the following state-space model for area i.

$$\begin{cases} \dot{x}(t) = Ax(t) + Bu(t) + B_d w(t) \\ y(t) = Cx(t) \end{cases} \tag{2}$$

Considering the effect of integration of wind power into the power system and ACs participation uncertainties, a plant with the parameter uncertainties and external disturbance is given based on (2).

$$\begin{cases} \dot{x}(t) = (A + \Delta A)x(t) + (B + \Delta B)u(t) + B_d w(t) \\ y(t) = Cx(t) \end{cases} \tag{3}$$

where ΔA and ΔB are uncertainties.

2.2 Objective of this paper

For the LFC scheme integrated with wind power and ACs, this paper aims to maintain the frequency and tie-line power exchanges between different areas at the scheduled values by developing a robust EID-based controller. It can be described with the following problem. The external disturbances and parameter variations are lumped into a disturbance. Then, an observation mechanism is devised to estimate this lumped disturbance. Next, one signal that has the same effect on the system output as this disturbance is added to the input channel to compensate for their influence on the system's stability based on their estimates. Therefore, a robust EID-based LFC scheme is constructed that can tolerate the external disturbances, parameter uncertainties, and time delays and eliminate tracking errors.

2.3 EID-based robust LFC strategy

The LFC scheme aims to maintain the frequency and power interchanges with neighborhood areas at scheduled values. The increased wind power integrated into the power system reduces the usage of traditional generations while leading to low or zero inertia, which endangers the stable operation of the system. The ACs based DR resources are capable of accommodating intermittent wind power, but the ACs users' uncertain participation combines the inertia reduced by replacing conventional generators with wind turbines, leading to parameter uncertainties. As the EID-based control theory employs the two-degree of freedom control mode, it releases the constrains of the one-degree of freedom control structure. Moreover, it requires no inverse dynamics of the plant model to avoid the cancellation of unstable poles and zeroes for a nonminimum-phase plant.

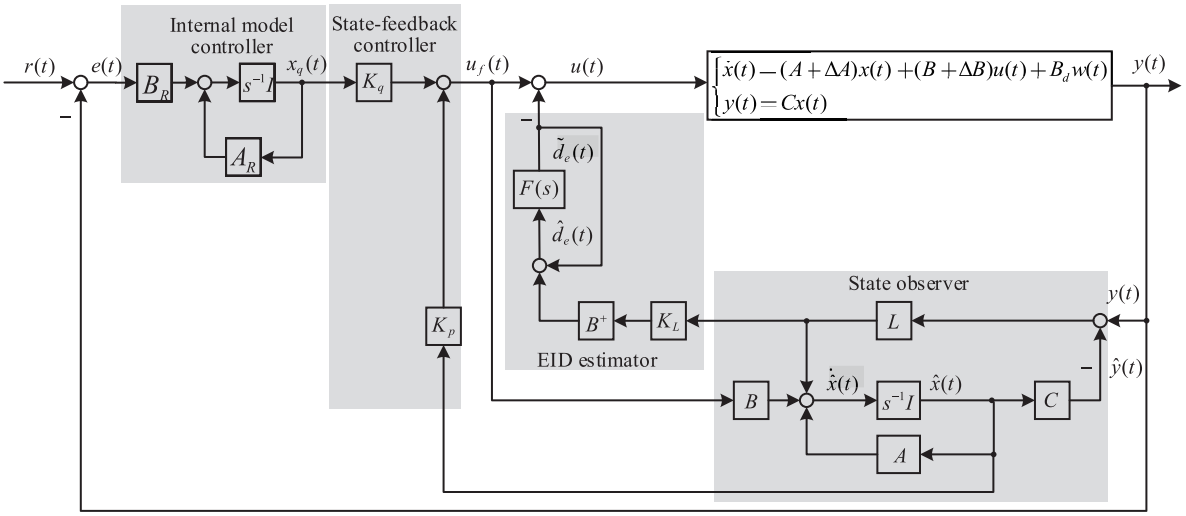

Figure 2 Configuration of EID-based LFC controller

Therefore, when the effects that the load variations, wind power fluctuations, and parameter uncertainties have on the frequency deviation are taken into account, the configuration of the EID-based control strategy is shown in Figure 2. This configuration contains the plant of the power system, an EID estimator, a Luenberger state observer, and a state-feedback controller. For the multi-area LFC scheme, the decentralized control method is applied by considering $\sum_{j=1,j\neq i}^{N} T_{ij}\Delta f_j$ as the disturbance of area i, which is also estimated by the EID estimator. Then, a control action is imposed on the control input based on the estimates to compensate for their influence, and the estimation accuracy plays a substantial role in realizing an improved disturbance-rejection performance. Therefore, compared with the conventional EID-based model, an extra gain matrix K_L is introduced into the EID estimator. This approach increases the flexibility of the system design and is helpful for constructing an EID-based LFC scheme with increased robustness against external disturbances as well as parameter uncertainties.

In (3), let the lumped disturbance be

$$d_l(t) = \Delta A x(t) + \Delta B u(t) + B_d w(t) \tag{4}$$

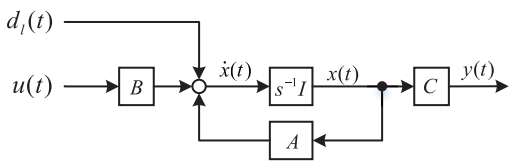

Figure 3 Plant

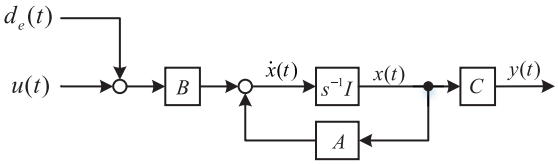

Figure 4 Plant with EID

Rewrite system (3) in Figure 3

$$\begin{cases} \dot{x}(t) = Ax(t) + Bu(t) + d_l(t) \\ y(t) = Cx(t) \end{cases} \tag{5}$$

The following assumption is made about plant (5).

Assumption 1: *(A,B,C)* is controllable and observable.

Assumption 2: *(A,B,C)* has no zeros on the imaginary axis.

We assume that one signal $d_e(t)$ is added to control input channel like Figure 4 in [28]. Thus, this plant can be expressed with

$$\dot{x}(t) = Ax(t) + B(u(t) + d_e(t)) \tag{6}$$

The definition of EID is given as follows.

Definition 1 [28]: Let the control input $u(t) = 0$. The output of plant (5) for the lumped disturbance $d_l(t)$ is $y_1(t)$. The output of plant (6) for the disturbance $d_e(t)$ is $y_2(t)$. If $y_1(t) \equiv y_2(t), t \geqslant 0$ holds, the disturbance $d_e(t)$ is called an EID of the lumped disturbance $d_l(t)$.

Lemma 1 [28]: Under Assumption 1 and 2, there always exists an EID $d_e(t) \in \Phi$ on the control input channel of the disturbance $d_l(t)$ imposed on plant (5), and the output it produces belongs to Φ with $\Phi = \{p_i(t)\sin(\omega_i t + \psi_i)\}, i = 0, ..., n, n < \infty$, and ω_i and ψ_i are constants, and $p_i(t)$ donates any polynomials in time $t (i = 0, ..., n)$.

In order to realize the effective disturbance rejection, a full-order state observer is constructed.

$$\begin{cases} \dot{\hat{x}}(t) = A\hat{x}(t) + Bu_f(t) + L(y - \hat{y}) \\ \hat{y}(t) = C\hat{x}(t) \end{cases} \tag{7}$$

where $L, \hat{x}(t), u_f(t)$ and $\hat{y}(t)$ are the observer gain, state, input and output, respectively.

Define the estimation error for the state as

$$\Delta x(t) = x(t) - \hat{x}(t) \tag{8}$$

and substitute it into (6) to develop

$$\dot{\hat{x}}(t) = A\hat{x}(t) + Bu(t) + \{Bd_e(t) + (A\Delta x(t) - \Delta\dot{x}(t))\} \tag{9}$$

Assume there exist a control input $\Delta w(t)$ satisfying

$$B\Delta w(t) = A\Delta x(t) - \Delta\dot{x}(t) + (K_L - I)LC\Delta x(t) \tag{10}$$

Let the estimate of the EID be

$$\hat{d}_e(t) = \Delta w(t) + d_e(t) \tag{11}$$

Combining (9), (10) and (11) yields

$$\dot{\hat{x}}(t) = A\hat{x}(t) + B(u(t) + \hat{d}_e(t)) - (K_L - I)LC\Delta x(t) \tag{12}$$

When comparing with equations (7) and (12), we can derive the following estimation of the EID.

$$\hat{d}_e(t) = u_f(t) - u(t) + B^+ K_L LC\Delta x(t) \tag{13}$$

where $B^+ = (B^T B)^{-1} B^T$.

In Figure 2, block $F(s)$ represents a low-pass filter and is employed to filter $\hat{d}_e(t)$ such that the noise can be filtered out to obtain the filtered disturbance estimate $\tilde{d}_e(t)$. This block satisfies

$$|F(jw)| \approx 1 \ \forall w \in [0, w_r] \tag{14}$$

with w_r being the highest angular frequency for the estimation.

The state-space of $F(s)$ is described with

$$\begin{cases} \dot{x}_F(t) = A_F x_F(t) + B_F \hat{d}_e(t) \\ \tilde{d}_e(t) = C_F x_F(t) \end{cases} \tag{15}$$

To let the power system's output track reference input $r(t)$, the internal model principle is alternative to realize the perfect tracking performance [35], and we have

$$\dot{x}_R(t) = A_R x_q(t) + B_R[r(t) - y(t)] \tag{16}$$

Also, the state-feedback control law is expressed with

$$u_f(t) = K_p\hat{x}(t) + K_q x_q(t) \tag{17}$$

where K_p and K_q are the control gains.

The control law becomes

$$u(t) = u_f(t) - \tilde{d}_e(t) \tag{18}$$

Remark 1. The parameter uncertainties and external disturbances are lumped to form a fictitious disturbance variable $d_l(t)$. The control law (18) suppresses the lumped disturbance $d_l(t)$ by constructing an observation mechanism to estimate $d_l(t)$ and taking a control action to compensate for its effect on the output based on its estimation. Thus, the disturbance-rejection performance can be realized.

Remark 2. Compared with the methods proposed in [29] and [32], K_L is introduced into the EID estimator, and it is capable of adjusting $\triangle x(t)$ to get better disturbance-rejection performance. When $K_L = I$ is given, the EID estimator shown in Figure 2 is deduced to the conventional EID estimator [28]. The Luenberger state observer is employed in the presented EID-based control structure, which has fewer parameters to be determined in comparison with the GSO required in [30,32]. Moreover, the output of the multi-area power system is the area control error ACE_i, whose reference is zero. The external disturbances that come from wind power, load changes, and tie-line power changes for the multi-area system often fluctuate randomly and are not aperiodic signals. Therefore, to realize a good tracking performance, it is sufficient to employ the internal model controller in this paper. The modified repetitive controller [29] that has increased sensitivity to aperiodic signals is possible to amplify the aperiodic disturbances and uncertainties rather than rejecting them.

3 Analysis and design of the EID-based LFC scheme

The closed-loop system in Figure 1 can be equivalently separated into two subsystems as shown in Figure 5, i.e., subsystem 1 and subsystem 2. Based on the separation theorem [33], subsystem 1 and subsystem 2 can be designed independently. To derive stability criteria for the EID-based LFC scheme, we let input reference $r(t) = 0$ and lumped disturbance $d_l(t) = 0$ and obtain

$$\begin{cases} \dot{x}(t) = Ax(t) + Bu(t) \\ y(t) = Cx(t) \end{cases} \tag{19}$$

From (8), (15), (17),(18) and (19), we have

$$\dot{x}(t) = (A + BK_p)x(t) + BK_q x_q(t) - BK_p \Delta x(t) - BC_F x_F$$

Substituting (19) into (16) yields

$$\dot{x}_q(t) = -B_R C x(t) + A_R x_q(t)$$

Combining (7), (8), (15), (17) and (19) leads to

$$\Delta \dot{x}(t) = (A - LC)\Delta x(t) - BC_F x_F$$

Adding (13) into (16) enables the following relationship

$$\dot{x}_F(t) = (A_F + B_F C_F)x_F(t) + L_0 \Delta x(t)$$

where $L_0 = B_F B^+ K_L L$.

3.1 Analysis and design of state feedback controller in subsystem 1

Define $\varphi_1^T(t) = [x^T \ x_q^T]$. For analyzing the internal stability of subsystem 1, its state-space model is

$$\dot{\varphi_1}(t) = \begin{bmatrix} A + BK_p & BK_q \\ -B_R C & A_R \end{bmatrix} \varphi_1(t) \tag{20}$$

The following theorem is given to guarantee the asymptotic stability of subsystem 1, which can be used to adjust the gains of the feedback controller according to the value of scalar a.

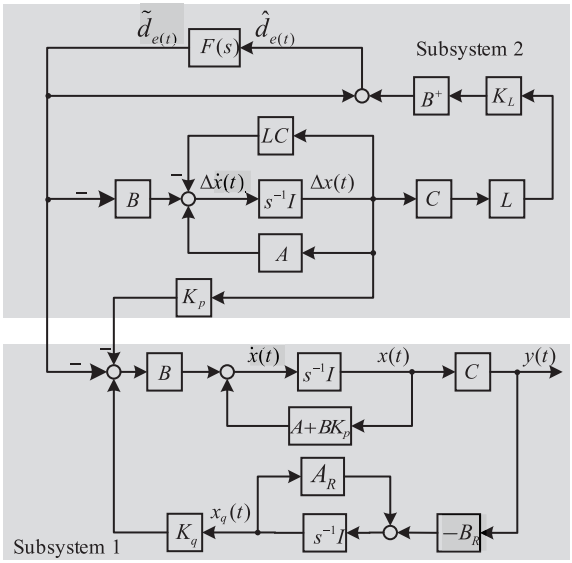

Figure 5 Equivalent system of Figure 2 with $r(t) = 0$ and $d_l(t) = 0$

Theorem 1. For given scalar a, system (20) is asymptotically stable, if there exist symmetrical positive-definite matrix P_1, and appropriately dimensioned matrices M_1 and V, such that the following inequality holds

$$\Xi_1 < 0 \tag{21}$$

where

$$\Xi_1 = 2e_1^T P_1 e_2 + 2[e_1^T \ e_2^T] \begin{bmatrix} I \\ aI \end{bmatrix} \left(M_1 e_2 - \begin{bmatrix} A & 0 \\ -B_R C & A_R \end{bmatrix} M_1 e_1 - \begin{bmatrix} B \\ 0 \end{bmatrix} V e_1 \right)$$
$$e_i = \left[0_{n\times(i-1)n}, I_{n\times n} \right], i = 1, 2$$

Then, the gains of the feedback controller are given by

$$[K_p | K_q] = V M_1^{-1} \tag{22}$$

The proof of Theorem 1 is given in Appendix B.

3.2 Analysis and design of state observer and EID estimator in subsystem 2

For subsystem 2, define $\varphi_2^T(t) = [\Delta x^T \ x_F^T]$, and consider its internal stability. Then, its state-space model is established with

$$\dot{\varphi_2}(t) = \begin{bmatrix} (A - LC) & -BC_F \\ L_0 C & A_F + B_F C_F \end{bmatrix} \varphi_2(t) \tag{23}$$

A sufficient condition for the asymptotical stability of subsystem 2 is derived below. Therefore, the gains of the EID-based estimator can be developed.

Theorem 2. For given scalar b, system (23) is asymptotically stable, if there exist symmetrical positive-definite matrix P_2, and appropriately dimensioned matrices N_{11}, N_{22}, W_1, and W_2, such that the following inequality holds

$$\Xi_2 < 0 \tag{24}$$

where

$$\Xi_2 = 2\tilde{e}_1^T P_2 \tilde{e}_2 + 2[\tilde{e}_1^T \ \tilde{e}_2^T] \begin{bmatrix} I \\ bI \end{bmatrix} \left(\begin{bmatrix} N_{11} & 0 \\ 0 & N_{22} \end{bmatrix} \tilde{e}_2 - \begin{bmatrix} N_{11} & 0 \\ 0 & N_{22} \end{bmatrix} \begin{bmatrix} A & -BC_F \\ 0 & A_F + B_F C_F \end{bmatrix} \tilde{e}_1 - \begin{bmatrix} -W_1 C & 0 \\ W_2 C & 0 \end{bmatrix} \tilde{e}_1 \right)$$

$\tilde{e}_i = \left[0_{n\times(i-1)n}, I_{n\times n}\right], i = 1, 2$

Hence, in subsystem 2, the gains of the observer and the EID-based estimator can by calculated respectively by

$$L = N_{11}^{-1}W_1, L_0 = N_{22}^{-1}W_2, K_L = BB_F^{-1}L_0L^+ \tag{25}$$

The proof of Theorem 2 is given in Appendix B.

When K_L is replaced with I, the IEID estimator reduces to the conventional one. The following corollary is then established to facilitate the design of controller gain L for the conventional estimator.

Corollary 1. For given scalar c, system (23) is asymptotically stable, if there exist symmetrical positive-definite matrix P_3, and appropriately dimensioned matrices X_{11}, X_{22}, W_3, and N_{44}, such that the following inequality holds

$$\Xi_3 < 0 \tag{26}$$

where

$$\Xi_3 = 2\bar{e}_1^T P_3 \bar{e}_2 + 2[\bar{e}_1^T \ \bar{e}_2^T] \begin{bmatrix} I \\ cI \end{bmatrix} \left(\begin{bmatrix} N_{33} & 0 \\ 0 & N_{44} \end{bmatrix} \bar{e}_2 - \begin{bmatrix} A & -BC_F \\ 0 & A_F+B_FC_F \end{bmatrix} \begin{bmatrix} N_{33} & 0 \\ 0 & N_{44} \end{bmatrix} \bar{e}_1 - \begin{bmatrix} -W_3C & 0 \\ B_FB^+W_3C & 0 \end{bmatrix} \bar{e}_1 \right)$$

$\bar{e}_i = \left[0_{n\times(i-1)n}, I_{n\times n}\right], i = 1, 2$

where

$$N_{33} = V \operatorname{diag}\{X_{11}, X_{22}\} V^{\mathrm{T}} \tag{27}$$

with V defined in the singular value decomposition (SVD) of output matrix C [39]. Here,

$$C = U \begin{bmatrix} D & 0 \end{bmatrix} V^{\mathrm{T}}$$

Thus, controller gain L can by calculated by

$$L = W_3UDX_{11}^{-1}D^{-1}U^{-1} \tag{28}$$

The proof of Corollary 1 is simple and here is omitted.

Remark 3. Theorem 2 and Corollary 1 are derived to develop the controller gains required by the EID estimator in this paper and the conventional one. Comparing with N_{11} in linear matrix inequality (LMI) (24), there is an extra constraint imposed on N_{33} in LMI (26), i.e., matrix N_{33} must be given a specific structure similar to equation (27). Therefore, by introducing K_L into the EID estimator, the increasing relax matrices are introduced to form a stability criterion that is conservatism-reduced and is expected to develop controller gains with a better dynamic performance. Moreover, the number of decision variables contained in Theorem 2 is similar to that required by Corollary 1. That is, even though Theorem 2 is derived with more degrees of freedom, its computational burden is not increased in comparison with that of Corollary 1.

Remark 4. It is known that the real world power system is large-scale and its state-space model is often high-dimensional. Hence, we have to consider the computational burden when designing the controllers through the Lyapunov theory. In this paper, based on the separation theorem, Subsystems 1 and 2 can be designed independently, i.e., Theorem 1 and Theorem 2 provide sufficient conditions that guarantee the asymptotic stability of Subsystem 1 and Subsystem 2, respectively. Since both the order of Subsystems 1 and 2 is reduced by half, the dimension of the LMIs used for calculating controller gains is reduced accordingly. Thus, the controller gains can be designed with less time consumption, which prompts the application of stability criteria established for realizing controller design in a practical power system effectively.

3.3 Summary of analysis steps

The detailed implementation of the developed method is summarized as follows.

Step1. Model establishment. The state-space model of the open-loop LFC considering wind power and a loop of the ACs is obtained. Then, a closed-loop LFC scheme is modelled by employing an EID-based controller.

Step2. Controller design. The closed-loop system established is divided into two subsystems where the gains of the feedback controller and EID estimator are determined independently.

Step3. Simulation verification. Simulation studies are performed to verify the effectiveness and improvements of the proposed method.

4 Case studies

Case studies are based on the single-area and two-area LFC schemes. They aim to demonstrate that the proposed EID-based controllers present an improved robustness against external disturbances, parameter variations, and time delays when compared with the decay-rate based PID-type controllers [20], adaptive fuzzy control [21] and conventional EID-based method [28]. Each area of the LFC scheme is assumed to have an equivalent generator, and the parameters of the LFC schemes can be found in Appendix A. The actual values for T_g, T_t, D, M, and R are assumed to change between the range of $1 + \Delta(\%)$ times the typical values such that different degree of parameter uncertainties for the LFC scheme are reflected in parameter variation (PV) by $\Delta(\%), \Delta \in [-25\%, -15\%, 0, 15\%, 25\%]$. The simulation studies are carried out following Figure 1, and some nonlinearities are added, including the generation rate constraint (GRC).

4.1 Single-area LFC scheme

1) Controller design: To select the optimal tuning parameters, a and b, and optimize the controller gains, we introduce a performance index, the integral of the time multiplied absolute value of the error (ITAE), to evaluate the overall performance of the EID-based method in Figure 2 and establish a design optimization.

For the single-area LFC scheme, we form the following optimization problem

$$\begin{cases} ITAE = \int_0^{50} t \mid ACE \mid dt \\ \min \ ITAE \ \text{ subject to } \ \text{LMIs (21) and (24)} \end{cases} \tag{29}$$

Theorem 1 and Theorem 2 employ two tuning parameters a and b. We tune a and b to find feasible solutions for both LMIs (21) and (24). Hence, we can obtain the gains of the feedback controller contained in subsystem 1 based on equation (22) while the observer and EID estimator gains of subsystem 2 are developed through (25). To realize a satisfactory robust control performance, the PSO algorithm is chosen to adjust these two parameters to solve optimization problem (29). The detailed implementation of the PSO algorithm refers to [36]. Finally, we get the optimized parameters $a = 0.017$ in Theorem 1 and $b = 0.018$ in Theorem 2. The gains required in the EID-based controller are listed in Table 3 (donated C_1).

2) Simulation verification: To show that the developed EID-based controllers have an increased dynamic performance compared with the existing decay-rate based PID controller (denoted C_2), adaptive fuzzy control (denoted C_3) and conventional EID-based method (denoted C_4) in terms of robustness against random disturbance and parameter uncertainties as well as time delays, three scenarios are designed to test the closed-loop one-area power system equipped with different controllers. The GRC is assumed to be ± 0.1 pu/min.

For scenario 1. The presence of random fluctuation changes for the load and wind power are applied to the single-area system. They are depicted in Figure 6. Then, the system responses are recorded in Figure 7, where the random changes, the frequency derivations, and the ACEs are included. Based on

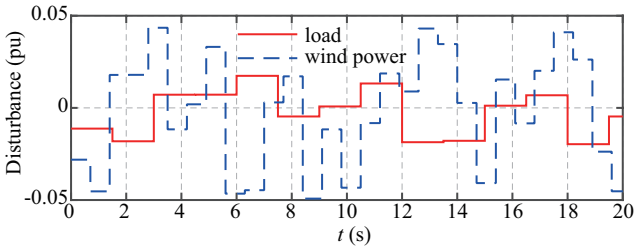

Figure 6 Random load changes and wind power fluctuations assumed for scenario 1

these results, the EID-based controller allows a smaller frequency deviation than those of the other three types of controllers, when the external disturbances are injected in the power system.

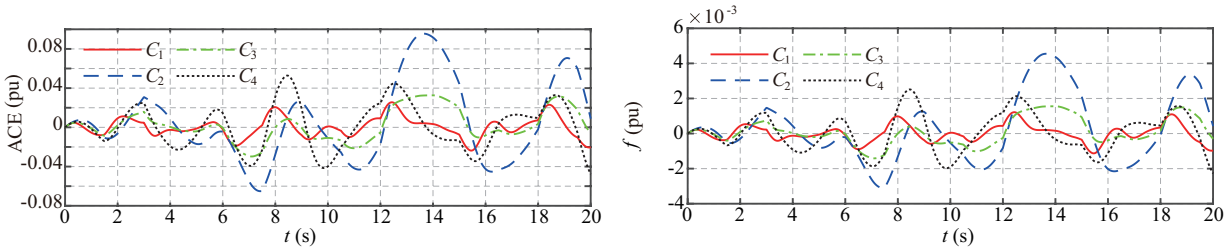

Figure 7 System responses of single-area LFC scheme with different controllers for scenario 1

Figure 8 compares the tracking errors when the LFC system is equipped with controllers C_1, C_2, C_3 or C_4, and random wind power and load changes are assumed. As shown, the peak-to-peak tracking error for the EID-based method C_1 presented in this paper is the smallest among the four methods. By contrast, the decay-rate based PID controller C_2 leads to the largest tracking error in the LFC system with a random external disturbance.

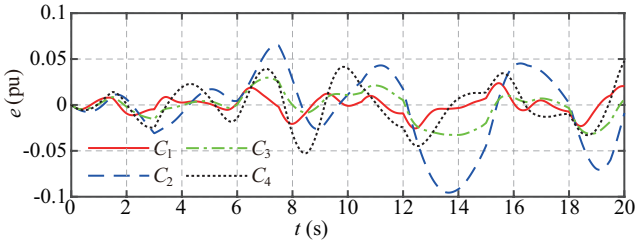

Figure 8 Tracking errors of single-area LFC scheme with different controllers for scenario 1

For scenario 2. When there are uncertainties in the system parameters ($\Delta \in [-25\%, -15\%, 0, 15\%, 25\%]$), the dynamic performances of the LFC scheme controlled by the EID controller, decay rate-based PID controller, adaptive fuzzy control, and the conventional EID-based controller are tested, respectively. This scenario aims to show that although these four controllers are designed based on the standard parameters, the EID-based controller has the best capability of compensating the lumped disturbance combined with external disturbances for the LFC scheme despite parametric variations. Here, for the single-area LFC scheme, the figure of demerit (FD) [37] is defined as

$$FD = (OS \times 10)^2 + (FU \times 4)^2 + (T_s \times 0.3)^2 \tag{30}$$

where OS, FU and T_s represent the overshoot, first undershoot and settling time of the frequency deviation of the single-area LFC system, respectively. The indexes of FD and ITAE are used to evaluate the dynamic performances of the considered controllers. In this case, the step changes of wind power and load disturbance with 0.1 pu and 0.05 pu amplitudes, respectively, are assumed in the single-area LFC scheme. Then, the dynamic responses of the power system are shown with the results listed in

Table 1, where the FD and ITAE mentioned above are included. This table indicates that although the four related controllers contain robustness against parameter uncertainties, under the same situation, the EID-based controller realizes the best dynamic performance, which contributes to the system stability.

Table 1 Performance indices of ITAE and FD for both single-area and two-area

	Single-area								Two-area							
	ITAE				FD				ITAE				FD			
$PV(\%)$	$\boldsymbol{C_1}$	C_2	C_3	C_4	$\boldsymbol{C_1}$	C_2	C_3	C_4	$\boldsymbol{C_5}$	C_6	C_7	C_8	$\boldsymbol{C_5}$	C_6	C_7	C_8
-25	**0.4**	1.8	2.9	1.2	**4**	10	49	16	**3**	9	7	11	**14**	16	19	15
-15	**0.3**	1.8	3.4	0.7	**2**	12	91	8	**4**	10	8	13	**15**	17	21	18
0	**0.3**	2	2.5	0.3	**2**	13	215	3	**5**	10	12	22	**14**	20	26	31
15	**0.4**	1.9	3.5	1.2	**2**	13	133	2	**8**	13	18	19	**22**	33	36	45
25	**0.6**	2.2	2.4	1.6	**14**	22	23	23	**11**	19	27	28	**31**	50	44	45

For a parameter variation equal to -25%, we depict the curves of the tracking errors for the four methods considered in Figure 9. From this figure, we find that when the LFC system uses the EID-based controller developed in this paper, its tracking error still converges quickly even though the level of parameter variation reaches -25%.

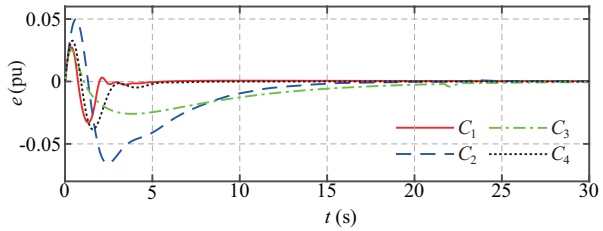

Figure 9 Tracking errors of single-area LFC scheme with different controllers for scenario 2 (-25% PV

For scenario 3. Both the LFC scheme and the aggregation of ACs use the communication channels to transmit the measurements and control commands, which introduces time delays [38]. In this paper, the four considered controllers are designed without considering the time delays. Therefore, this case is designed to verify that the proposed EID-based controller has a higher tolerance for the effect of time delay than those of the other three methods. The wind power and load disturbance with 0.1 pu and 0.05 pu step changes, respectively, are applied to the single-area LFC scheme again. For comparison, assuming there is no time delay appearing in the network channels at first, the LFC scheme's dynamic responses are shown in Figure 10 (a). Then, the random delays equal to $[0, 300]$ ms appear in both the control input channel and the ACs participation loop, and the dynamic performances of the power system are changed from those of Figure 10 (a) to those of Figure 10 (b). These simulation results indicate that the dynamic performance of the EID-based controller C_1 changes with the increase in the time delay. However, it still maintains the best robustness against time delays in comparison with the decay rate-based PID controller C_2, adaptive fuzzy control C_3, and conventional EID-based method C_4 .

Similarly, with the introduction of a time delay, based on Figure 11, the peak-to-peak tracking error is increased to 0.08 pu when the LFC scheme is equipped with controller C_1, and it is slightly bigger than those of the controller C_2 based system. However, for C_1, less than 15 s is consumed on converging to zero states, which is the fastest speed among the four controllers.

4.2 Two-area LFC scheme

1) Controller design: To improve the dynamic performance of the designed EID-based controller, for the multi-area LFC system, the index of ITAE contained in optimization problem (29) needs to be redefined

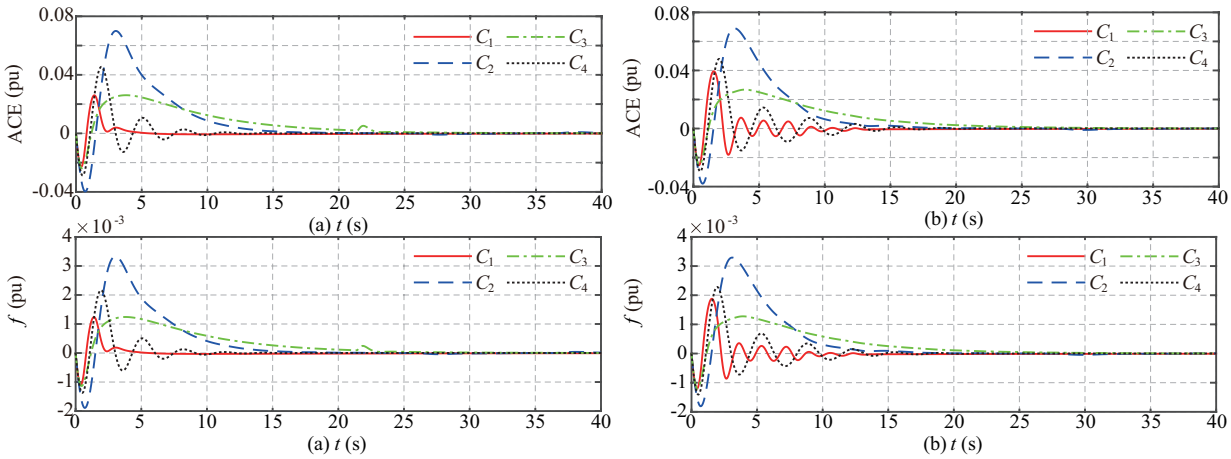

Figure 10 System responses of single-area LFC scheme with different controllers for scenario 3. (a) without time delay, (b) random delay

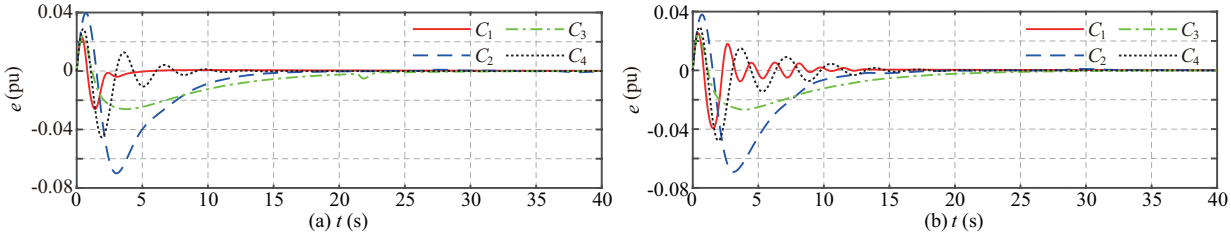

Figure 11 Tracking errors of single-area LFC scheme with different controllers for scenario 3. (a) without time delay, (b) random delay

as

$$ITAE = \sum_{i=1}^{N} \int_{0}^{50} t \mid ACE_i \mid dt$$

When the EID-based LFC controller is unresolved for the two-area power system, the decentralized-type controller is an alternative for shortening the process of optimizing controller gains. The tie-line power changes between the neighboring control areas are regarded as an external disturbance. In addition, the controller gains are tuned under the average system parameters. Following the same steps as those for designing the controller in the one-area LFC scheme, we finally obtain that when tuning the parameters $a = 4.81$ and $b = 0.47$ are given in the PSO algorithm, both LMIs (21) and (24) are feasible, and index ITAE is minimized. Therefore, the desired controller gains for the EID-based LFC scheme are calculated based on (22) and (25), and they are expected to have the optimized dynamic performance. The controller values are listed in Table 4.

2) Simulation verification: The closed-loop two-area power system is equipped with the proposed EID-based controller (denoted C_5), the decay-rate based PID-type controller (denoted C_6), the adaptive fuzzy controller (denoted C_7), and the conventional EID-based controller (denoted C_8). Similarly, to further verify that the developed EID-based LFC scheme has an improved robustness, a second case study is performed under the following three scenarios. The GRC is assumed to be ± 0.1 pu/min.

For scenario 4. The random load and wind power changes representing the expected fluctuations from load demand and wind power depicted in Figure 12 are assumed to appear in both areas. The dynamic responses of the two-area LFC scheme equipped with different controllers are also recorded, and include the random changes, the ACEs, and the tie-line power changes. From these results, by compensating for the influence that external disturbances have on the control output over time, the EID-based controller C_5 can always make the two-area system stable. By contrast, the decay-rate based PID controller C_6, adaptive fuzzy controller C_7 and conventional EID-based controller C_8 can barely address these external

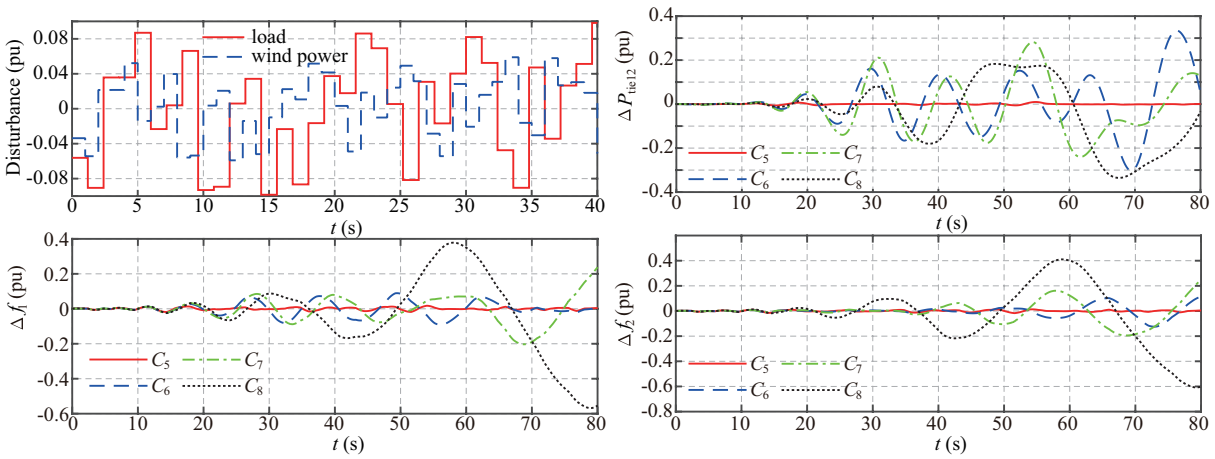

Figure 12 System responses of two-area LFC scheme with different controllers for scenario 4

disturbances. As a result, the LFC scheme under these three controllers finally loses its frequency stability. This case further demonstrates the proposed EID-based controller has a better capability for tolerating the load disturbance, wind power, and tie-line power changes when compared with the existing three kinds of controllers.

Under this scenario, the tracking errors for the two-area LFC scheme are described in Figure 13 when it is tested under different controllers. The red line expresses the tracking error of the system controlled by C_5, and there is no divergence, which shows that the presented EID-based LFC scheme realizes both satisfactory tracking control performance and disturbance-rejection performance. The other three lines represent the tracking results obtained by C_6, C_7 and C_8. They can not suppress the external disturbances as well as the tie-line power changes.

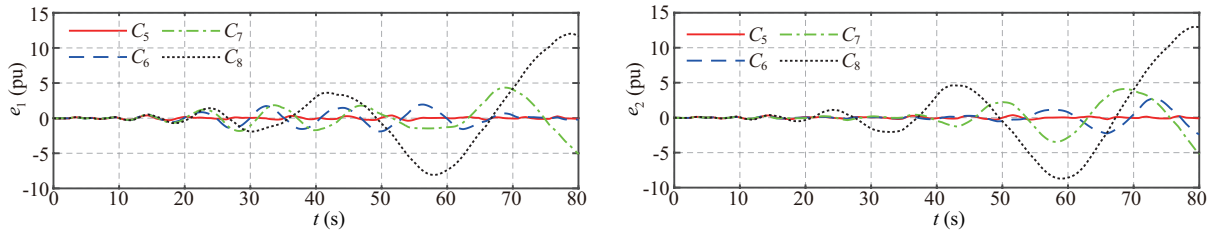

Figure 13 Tracking errors of two-area LFC scheme with different controllers for scenario 4

For scenario 5. There exist parameter uncertainties (within ±25%). The robustness of the four comparative controllers against the parameter uncertainties is checked. The step changes of load demand and wind power are applied to each area, i.e., $\Delta P_{L1} = 0.2$ pu, $\Delta P_{L2} = 0.2$ pu, $\Delta P_{w1} = 0.1$ pu, and $\Delta P_{w2} = 0.1$ pu. For multi-area LFC scheme, the FD can be defined as

$$FD = \sum_{i=1}^{N} \left[(OS_i \times 10)^2 + (FU_i \times 4)^2 + (T_{si} \times 0.3)^2 \right] \tag{31}$$

where OS_i, FU_i, T_{si} and N donate the the overshoot, first undershoot, settling time of the frequency deviation of area i and the number of areas, respectively. The variation tendency of system frequency is depicted with indices ITAE and FD in Table 1. As we can see, in the same case, the lowest values for ITAE and FD are obtained for the EID-based LFC scheme in comparison with those derived from the LFC system equipped with the decay rate-based PID controller, adaptive fuzzy controller or the conventional EID-based controller.

We also display the tracking errors of the two-area LFC scheme with different controllers in Figure 14 for a -25% parameter variation. Considering the first area, the peak to peak tracking error for C_5 is near

0.36 pu, and it is the smallest when compared with the results for C_6, C_7 and C_8. Additionally, using the developed EID-based controller, the tracking error can be eliminated more effectively.

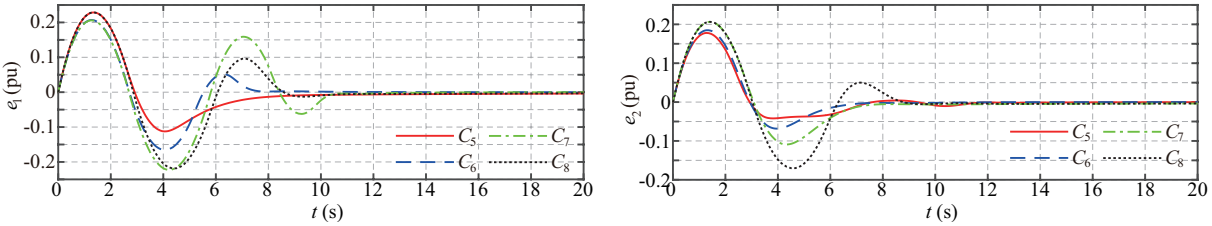

Figure 14 Tracking errors of two-area LFC scheme with different controllers for scenario 5 (-25%)

For scenario 6. First, the same step load and wind power are introduced into the two-area LFC scheme as those of scenario 5, while no time delays are considered. Figure 15 (a) shows the dynamic responses of the LFC system with different controllers. Then, the time delays considered with random delays equal to 500 ms are assumed to arise from the channels of control input and ACs participation in the two-area power system whose dynamic performances are shown in Figure 15 (b). It is shown that the EID-based controller C_5 presented in this paper and the conventional EID-based controller C_8 can stabilize the system frequency. Moreover, C_5 still behaves better robustness against time delays and disturbance-rejections than C_8. In contrast, the decay rate based PID controller C_6 and the adaptive fuzzy controller C_7 cannot depress the fluctuation of frequency.

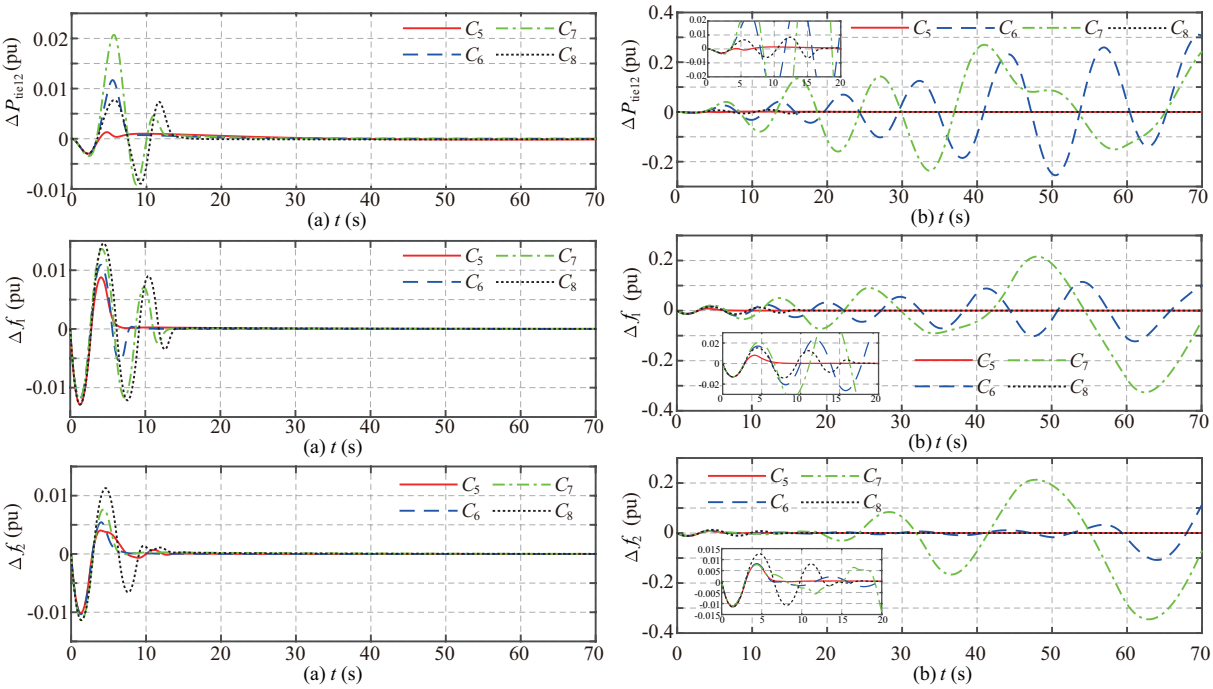

Figure 15 System responses of two-area LFC scheme with different controllers for scenario 6. (a) without time delay, (b) random delay

Figure 16 shows the tracking errors for the two-area system with and without a time delay. When no time delay is considered, the peak to peak tracking errors for C_5-based LFC system are 0.45 pu in area 1 and 0.3 pu in area 2, which are smaller compared with those obtained for the system equipped with controllers C_6, C_7 or C_8. The introduction of the time delay makes the decay-rate based controller C_6 and adaptive fuzzy controller C_7 unable to eliminate the tracking errors. Whereas, the EID-based controllers C_5 and C_8 remain robust to time delays. The former controller presented in this paper realizes lower peak to peak tracking errors and requires less time to eliminate the tracking errors. Thus, the improved

robustness against time delays of the developed EID-based LFC scheme is verified.

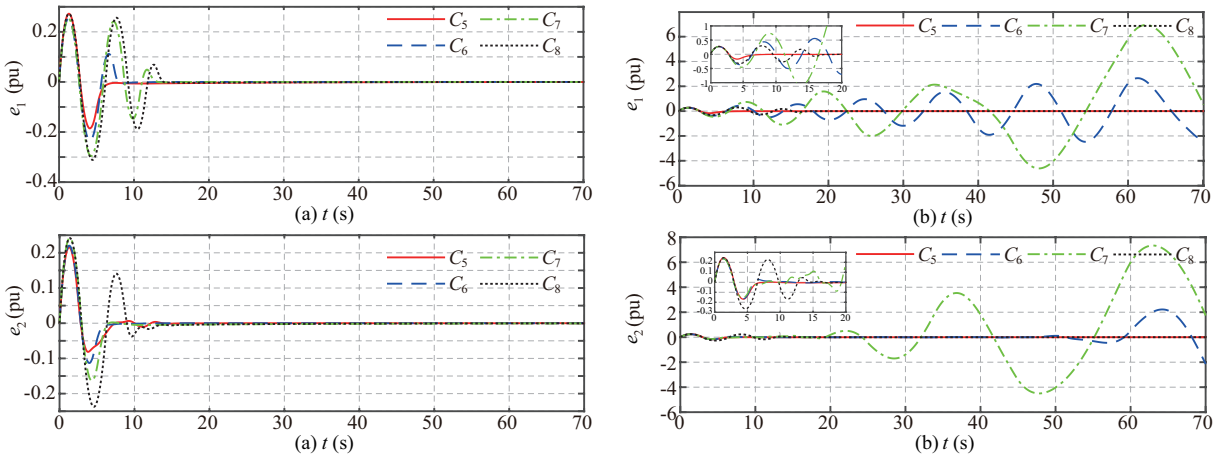

Figure 16 Tracking errors of two-area LFC scheme with different controllers for scenario 6. (a) without time delay, (b) random delay

5 Conclusion

This paper has developed an EID-based LFC scheme for the ACs participating in the power system integrated with wind power. The parameter uncertainties and external disturbance has been lumped into a fictitious disturbance to be estimated by an EID estimator. By imposing an estimate of the disturbance into the control input, the disturbance-rejection performance for the LFC scheme has been achieved. Based on the Lyapunov theory and the separation theorem, the feedback controller and the EID estimator have been designed independently in terms of linear-matrix-inequalities. By adjusting the tuning parameters, the controller gains have been optimized while minimizing the index that is the integral of the time multiplied absolute value of the error. Case studies have been carried out for the one-area and two-area power systems. The simulation results have verified that the obtained controllers have an improved robustness against parameter uncertainties, stochastic disturbances, and time delays.

In this paper, a Luenberger observer has been utilized to produce an estimate of the EID, based on which a control action is taken to compensate for its influence on the output. Note that the Luenberger observer has only a proportional loop. To further improve the estimation accuracy of the state variables, additional feedback could be added, e.g., an integral controller could be introduced to form a proportional-integral observer. By introducing an extra controller gain, the flexibility of system design is increased to improve the dynamic disturbance-rejection performance of the developed controllers. Moreover, theoretical analysis and explanation for the robustness of the designed controllers are desired but challenging. Providing a theoretical basis for determining the limits and ultimate performance of the developed control systems would be of great significance. These works will be investigated in the near future.

Appendix A.

The parameters used in the one-area and two-area LFC schemes are shown in Table 2. Also, the gains of the EID-based LFC scheme determined in this paper as well as the controller parameter developed with the decay-rate based method are shown in the following two tables, where Tables 3 and 4 are listed for the one-area and two-area systems, respectively.

Table 2 Two-area LFC scheme considering wind power and the ACs loop

Parameters	T_t	T_g	R	D	β	M	c_p	m	k	d_{ac}	EER	T_{12}
Area1	0.30	0.10	0.05	1.00	21.0	10	1.01	0.25	8	0.025	3.75	0.1968
Area2	0.40	0.17	0.05	1.50	21.5	12	1.01	0.25	15	0.015	3.75	0.1968

Table 3 Controllers determined for one-area system by this paper and by the method in [20]

$$K_L = e^{-6}\begin{bmatrix} 0_{2\times5} \\ -0.0093\ -0.0002\ 0.2996\ -0.0005\ 0.0033 \\ 0_{2\times5} \end{bmatrix}$$

$$L = [0.2955\ 0.0049\ -9.5251\ 0.0152\ -0.1043]^T$$

$$K_p = [-207.8956\ -3.5772\ -1.2557\ -4.5032\ 5.5627]$$

$$K_q = 1.5853$$

Table 4 Controllers determined for two-area system by this paper and by the method in [20]

Area 1	Area 2
$K_{L1}=e^{-5}\begin{bmatrix} 0_{3\times6} \\ -0.0010\ -0.0012\ 0.0001\ 0.1890\ 0\ 0.0002 \\ 0_{2\times6} \end{bmatrix}$	$K_{L2}=e^{-5}\begin{bmatrix} 0_{3\times6} \\ 0.0025\ 0.0021\ -0.0002\ -0.1981\ 0\ -0.0008 \\ 0_{2\times6} \end{bmatrix}$
$L_1=[0.0482\ 0.0609\ -0.0046\ -9.5041\ 0.0017\ -0.0082]^T$	$L_2=[0.0686\ 0.0591\ -0.0055\ -5.4644\ 0.0004\ -0.0232]^T$
$K_{p1}=[-25.0580\ -0.6304\ -0.7113\ 0.1324\ -1.3190\ 1.6173]$	$K_{p2}=[-51.2391\ -0.9185\ -1.3158\ -0.2084\ -2.0945\ 2.5513]$
$K_{q1}=0.1052$	$K_{q2}=0.1544$

Appendix B.

Proof of Theorem 1

Proof: Choose the following Lyapunov function:

$$V_1(t) = \varphi_1^T(t) P_1 \varphi_1(t) \tag{32}$$

with positive-definite matrix P_1 to be determined.

Calculating the derivative of $V_1(t)$ yields

$$\dot{V}_1(t) = 2\varphi_1^T(t) P \dot{\varphi}_1(t) \tag{33}$$

System equation (20) is described with the following zero equation.

$$0 = 2[\varphi_1\ \dot{\varphi}_1] M \left(\dot{\varphi}_1 - \begin{bmatrix} A & 0 \\ -B_R C & A_R \end{bmatrix} \varphi_1 - \begin{bmatrix} B \\ 0 \end{bmatrix} [K_p\ K_q] \varphi_1 \right) \tag{34}$$

with $M = \begin{bmatrix} M_1' \\ aM_1' \end{bmatrix}$ and M_1' is the appropriately dimensioned matrix.

Combine equations (33) and (34), and then pre- and post-multiply $\mathrm{diag}\{M_1'^{-1}, M_1'^{-1}\}$. Let $M_1'^{-1} = M_1$ and $[K_p\ K_q]M_1 = V$. It is clear that the holding of LMI-based condition in Theorem 1 leads to $V_1(t) > 0$ and $\dot{V}_1(t) \leqslant -\varepsilon_1 \|\varphi_1(t)\|^2$ for a sufficient small scalar $\varepsilon_1 > 0$, which shows the asymptotical stability of the first subsystem (20).

Proof of Theorem 2

Proof: Choose the following Lyapunov function:

$$V_2(t) = \varphi_2^T(t) P_2 \varphi_2(t) \tag{35}$$

with positive-definite matrix P_2 to be determined.

The derivative of $V_2(t)$ is

$$\dot{V}_2(t) = 2\varphi_2^T(t)P_2\dot{\varphi}_2(t) \tag{36}$$

Similarly, the following zero equation is used to describe system equation (23).

$$0=2[\varphi_2\ \dot{\varphi}_2]N\left(\dot{\varphi}_2-\begin{bmatrix}A & -BC_F\\ 0 & A_F+B_FC_F\end{bmatrix}\varphi_2-\begin{bmatrix}-LC & 0\\ L_0C & 0\end{bmatrix}\varphi_2\right) \tag{37}$$

Combine equations (36) and (37). Let $N=\begin{bmatrix}N_1\\ bN_1\end{bmatrix}$ with $N_1=\mathrm{diag}\{N_{11},N_{22}\}$, and$N_{11}L=W_1$, and $N_{22}L_0=W_2$, where matrices W_1 and W_2 are appropriately dimensioned. Hence, the LMI-based condition in Theorem 2 realizes $V_2(t)>0$ and $\dot{V}_2(t)\leqslant-\varepsilon_2\|\varphi_2(t)\|^2$ for a sufficient small scalar $\varepsilon_2>0$. Then, the asymptotical stability of the second subsystem (23) is guaranteed.

Acknowledgements This work was supported in part by the National Natural Science Foundation of China (Grant Nos. 61973284 and 61873347), by the Hubei Provincial Natural Science Foundation of China (Grant No. 2019CFA040), by the 111 project (Grant No. B17040), by the Program of China Scholarship Council (Grant Nos. 201706410037 and 201706410012), and by the Fundamental Research Funds for National Universities, China University of Geosciences (Wuhan).

References

1 H. Bevrani, J.H. Chow, A.M. Stankovic, D. Hill, "*Robust power system frequency control*," New York: Springer, 2014.
2 L. Jin, C.K. Zhang, Y. He, L. Jiang, M. Wu, "Delay-dependent stability analysis of multi-area load frequency control with enhanced accuracy and computation efficiency," *IEEE Transactions on Power Systems,* 34(5): 3687-3696, 2019.
3 M. Dreidy, H. Mokhlis, S. Mekhilef, "Inertia response and frequency control techniques for renewable energy sources: A review," *Renewable and Sustainable Energy Reviews,* 69: 144-155, 2017.
4 J.H. Li, J.Y. Wen, S.J. Cheng, H. Wei, "Minimum energy storage for power system with high wind power penetration usingp-efficient point theory," *Science China Information Sciences,* 57, 128202:1-12, 2014.
5 A. Latif, S.M. Suhail Hussain, D.C. Das, T.S. Ustun, "State-of-the-art of controllers and soft computing techniques for regulatedload frequency management of single/multi-area traditional and renewableenergy based power systems," *Applied Energy,* 266, 114858, 2020.
6 D.H. Tungadio, Y. Sun, "Load frequency controllers considering renewable energy integration in power system," *Energy Reports,* 5: 436-453, 2019.
7 S.A. Pourmousavi, M.H. Nehrir, "Introducing dynamic demand response in the LFC model," *IEEE Transactions on Power Systems,* 29(4): 1562-1572, 2014.
8 S. Wang, K. Tomsovic, "Fast frequency support from wind turbine generators with auxiliary dynamic demand control," *IEEE Transactions on Power Systems,* 34(5): 3340-3348, 2019.
9 V. Lakshmanan, M. Marinelli, J. Hu, H.W. Bindner, "Provision of secondary frequency control via demand response activation on thermostatically controlled loads: Solutions and experiences from Denmark," *Applied Energy*, 173: 470-480, 2016.
10 Q. Zhu, L. Jiang, W. Yao, C.K. Zhang, C. Luo, "Robust load frequency control with dynamic demand response for deregulated power systems considering communication delays," *Electric Power Components and Systems,* 45(1): 75-87, 2017.
11 N. Li, X.L. Wang, "Research of air conditioners providing frequency controlled reserve for microgrid," *Power System Protection and Control,* 43: 101-105, 2015.
12 C.W. Gao, Q.Y. Li, Y. Li, "Bi-level optimal dispatch and control strategy for air-conditioning load based on direct load control," *Proceedings of the CSEE*, 34: 1546-1555, 2014.
13 M. Liu, X.D. Chu, W. Zhang, "Cooperative generation-load frequency control strategy accounting for power network constraints," *Transactions of China Electrotechnical Society,* 31: 195-205, 2016.
14 X.Q. Hu, B.B. Wang, "A closed-loop control strategy for air conditioning loads to participate in demand response," *Energies*, 8: 1-28, 2015.
15 N. Nguyen, J. Mitra, "An analysis of the effects and dependency of wind power penetration on system frequency regulation," *IEEE Transactions on Sustainable Energy,* 7(1): 354-363, 2016.
16 Y. Li, P. Zhang, M. Althoff, M. Yue, "Distributed formal analysis for power networks with deep integration of distributed energy resources," *IEEE Transactions on Power Systems,* 34(6): 5147-5156, 2019.
17 C. Shen, Y. Bao, T. Ji, J. Zhang, Z. Wang, "A robust control strategy for air conditioner group to participate in power system frequency regulation," *2019 IEEE Innovative Smart Grid Technologies-Asia,* 678-682, 2019.
18 C. Mu, Y. Tang, H. He, "Improved sliding mode design for load frequency control of power system integrated an adaptive learning strategy," *IEEE Transactions on Industrial Electronics,* 64(8): 6742-6751, 2017.

19 H. Bevrani, M. R. Feizi, S. Ataee, "Robust frequency control in an islanded microgrid: H_∞ and μ-synthesis approaches," *IEEE Transactions on Smart Grid,* 7 (2): 706-717, 2016.

20 X.C. Shang-Guan, Y. He, C.K. Zhang, L. Jiang, J.W. Spencer, M. Wu, "Sampled-data based discrete and fast load frequency control for power systems with wind power," *Applied Energy*, 259, 114202, 2020.

21 K. Sabahi, S. Ghaemi, and M. Badamchizadeh, "Designing an adaptive type-2 fuzzy logic system load frequency control for a nonlinear timedelay power system," *Applied Soft Computing,* 43: 97-106, 2016.

22 C.J. Ramlal, A. Singh, S. Rocke, M. Sutherland, "Decentralized fuzzy H_∞ iterative learning LFC with time-varying communication delays and parameter uncertainties," *IEEE Transactions on Power Systems,* 34(6): 4718-4727, 2019.

23 W.H. Chen, J. Yang, L. Guo, S. Li, "Disturbance-observer-based control and related methods: An overview," *IEEE Transactions on Industrial Electronics,* 63 (2): 1083-1095, 2016.

24 E. Sariyildiz, R. Oboe, K. Ohnishi, "Disturbance observer-based robust control and its applications: 35th anniversary overview," *IEEE Transactions on Industrial Electronics,* 67 (3): 2042-2053, 2020.

25 S. Chen, W. Xue, S. Zhong, Y. Huang, "On comparison of modified ADRCs for nonlinear uncertain systems with time delay," *Science China Information Sciences,* 61, 070223:1-15, 2018.

26 L. Ren, C. Mao, Z. Song, F. Liu, "Study on active disturbance rejection control with actuator saturation to reduce the load of a driving chain in wind turbines," *Renewable Energy,* 133: 268-274, 2019.

27 H. Coral-Enriquez, J. Cortes-Romero, S.A. Dorado-Rojas, "Rejection of varying-frequency periodic load disturbances in wind-turbines through active disturbance rejection-based control," *Renewable Energy,* 141: 217-235, 2019.

28 J.H. She, M. Fang, Y. Ohyama, H. Hashimoto, M. Wu, "Improving disturbance-rejection performance based on an equivalent-input-disturbance approach," *IEEE Transactions on Industrial Electronics,* 55(1): 380-389, 2008.

29 L. Zhou, J.H. She, S.W. Zhou, C.Y. Li, "Compensation for state-dependent nonlinearity in a modified repetitive control system," *Int J Robust Nonlinear Control,* 1-14, 2017.

30 F. Liu, J. Ma, "Equivalent input disturbance-based robust LFC strategy for power system with wind farms," *IET Generation, Transmission and Distribution,* 12(20): 4582-4588, 2018.

31 P. Yu, M. Wu, J. She, K.Z. Liu, Y. Nakanishi, "An improved equivalent-input-disturbance approach for repetitive control system with state delay and disturbance," *IEEE Transactions on Industrial Electronics,* 65(1): 521-531, 2018.

32 L. Zhou, J.H. She, X.M. Zhang, Z.W. Cao, Z. Zhang, "Performance enhancement of RCS and application to tracking control of chuck-workpiece systems," *IEEE Transactions on Industrial Electronics,* 67(5): 4056-4065, 2020.

33 B.D.O. Anderson, J.B. Moore, *"Optimal controllinear quadratic methods,"* Englewood Cliffs, NJ: Prentice-Hall, 1989.

34 H. Hui, Y. Ding, Y. Song, S. Rahman, "Modeling and control of flexible loads for frequency regulation services considering compensation of communication latency and detection error," *Applied Energy*, 250: 161-174, 2019.

35 B.A. Francis, W.M. Wonham, "The internal model principle of control theory," *Automatica,* 12(5): 457C465, 1976.

36 H. Fan, L. Jiang, C.K. Zhang, C. Mao, "Frequency regulation of multi-area power systems with plug-in electric vehicles considering communication delays," *IET Generation, Transmission and Distribution,* 10(14): 3481-3491, 2016.

37 C.K. Zhang, L. Jiang, Q.H. Wu, Y. He, M. Wu, "Delay-dependent robust load frequency control for time delay power systems," *IEEE Transactions on Power Systems,* 28(3): 2192-2201, 2013.

38 S. Bhowmik, K. Tomsovic, A. Bose, "Communication models for third party load frequency control," *IEEE Transactions on Power Systems,* 19(1): 543-548, 2004.

39 P. Yu, M. Wu, J. She, Q. Lei, "Robust repetitive control and disturbance rejection based on two-dimensional model and equivalent-input-disturbance approach," *Asian Journal of Control,* 18(6): 2325-2335, 2016.